Intraday Volatility Patterns from Short-Dated Options*

Viktor Todorov† and Yang Zhang‡

April 7, 2024

Abstract

We propose a nonparametric estimator for the deterministic periodic component of volatility from short-dated options within an in-fill asymptotic setting. The estimator uses options with zero and one day to expiration sampled at high-frequency during a trading day. At each point in time, we aggregate the options to form nonparametric estimates of conditional risk-neutral expectations of future integrated return variation for the two available option tenors. A suitable ratio of these estimates removes the stochastic components of the conditional expectations of future volatility, up to asymptotically higher-order terms, and allows to form estimates of the deterministic periodic component of volatility. We derive a Central Limit Theorem for the estimator, with its rate of convergence determined from the mesh of the strike grid and the length of the time to expiration of the options. The newly-developed estimation procedure is applied to S&P 500 index options data.

Keywords: calendar effect, in-fill asymptotics, intraday volatility pattern, nonparametric volatility estimation, short-dated options.

JEL classification: C51, C52, G12.

*We would like to thank the Editor (Serena Ng), an Associate Editor and three anonymous referees for many useful comments and suggestions.

†Kellogg School of Management, Northwestern University; e-mail: v-todorov@northwestern.edu.

‡Financial Market Infrastructure Institution; e-mail: zhangyang360@gmail.com. Yang Zhang completed this work in her personal time. The views expressed in the article are the author's own and not those of her employer.

1 Introduction

A well-recognized and important feature of the volatility of most financial assets is its strong intraday periodic pattern, see e.g., Wood et al. (1985), Harris (1986), Admati and Pfleiderer (1988), Andersen and Bollerslev (1997, 1998) and Hong and Wang (2000), with volatility being much higher on average following market open and prior to market close than during the middle of the trading day. This intraday pattern of stochastic volatility is too large to be ignored and can have nontrivial effect on many estimation problems that involve the use of high-frequency data. For example, the nonparametric detection of jumps depends strongly on a good local estimator of volatility, which in turn depends on accounting for the intraday volatility pattern, see e.g., Boudt et al. (2011).

Earlier work has used both parametric and nonparametric methods for estimating the intraday periodic volatility component, see e.g., Andersen and Bollerslev (1997), Taylor and Xu (1997) and Boudt et al. (2011), among others. The nonparametric method, in particular, consists of forming local estimators of volatility during the day and then averaging the time series of these estimates. This estimation approach relies on a joint in-fill and long-span asymptotics.[1] Intuitively, the high-frequency data is needed for recovering nonparametrically volatility from stock returns while a long time span of the data set is needed in order to disentangle the stochastic (and stationary) component of volatility from the intraday periodic one. However, in a recent work, Andersen et al. (2019) show using a nonparametric test that the periodic component of volatility can change over time and Andersen et al. (2023) estimate its average value.

Given this evidence, the goal of this paper is to develop a nonparametric method for identifying the intraday periodic component of volatility without making use of long-span asymptotics. Such a method will avoid the need to use long time series of data and avoid either making an assumption that the intraday periodic component remains constant over time or modeling this time series variation via a parametric model.

Our method is based on short-dated options written on the asset, i.e., options that have short time to expiration and asymptotic expansions for risk-neutral variance measures constructed from them. As documented in Andersen et al. (2017), short-dated options have increased in popularity among investors over the last decade. Trading in such options has been facilitated by the introduction of the so-called weekly options which have weekly expiration cycle. For example, many stocks and indices have options, traded on the CBOE options exchange, that expire every Friday. Moreover, for options written on the S&P 500 index, starting from around the middle of 2022,

[1] One special situation in which long-span asymptotics will not be needed is if the stochastic component of volatility remains constant during the trading day, see Christensen et al. (2018).

CBOE offers options expiring on every day of the trading week. In Figure 1, we show the percentage of daily volume of S&P 500 index options traded on CBOE grouped by time to expiration. We consider only days on which options that expire on the same day (left plot) or on the following trading day (right plot) are available. As seen from the figure, a rather nontrivial percent of the total volume of traded S&P 500 index options is for ones with zero or one day tenor. These are the options that we are going to use in our analysis.

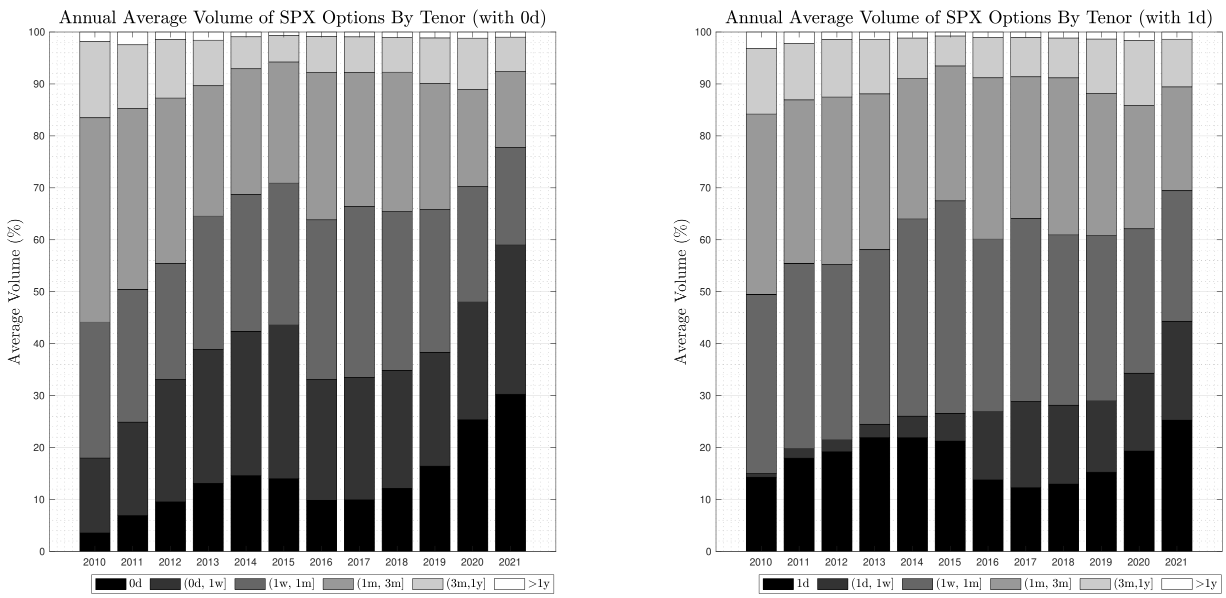

Figure 1: **S&P 500 Index Options Volume for 0-Day (left) and 1-Day (right) Tenor**. The left/right plot corresponds to days with options expiring on the same/next day.

Our estimator is built from measures of conditional risk-neutral expectations of future return variation for two short horizons measured at high-frequency during a trading day. These measures are constructed from portfolios of options with zero- and one-day tenor. Using short-time asymptotics, i.e., asymptotics for shrinking tenor of the options, we can proceed as if the stochastic components of volatility and jump intensity remain constant over the life of the options and equal to their value at the time of observing the option prices. Thus, the ratio of the risk-neutral volatility estimates over the two horizons, up to higher-order bias terms, does not depend on the stochastic components of volatility and jump intensity. Instead, its asymptotic limit is determined by functions of the deterministic periodic component of volatility we are after. By comparing such ratios at different parts of the trading day, we can estimate the intraday periodicity in volatility. Importantly, such estimators require that the periodic component of volatility is constant only over the short life of the options. This is in sharp contrast to return-based nonparametric estimates of these quantities that require that the periodic component of volatility remains constant throughout time.

We derive the rate of convergence of our estimator and provide an associated Central Limit Theorem (CLT). The asymptotic setup is of joint type: the mesh of the strike grids and the tenors of the options shrink simultaneously with the increase of the strike ranges of the options, which asymptotically converge to cover the whole positive part of the real line. The rate of convergence of the estimator is determined by both the mesh of the two strike grids as well as by the length of the two tenors. Its limiting behavior is governed by the options with strikes near the current underlying spot price, which in turn are dominated by the diffusive component of the spot price.

We evaluate the performance of our estimator on simulated data from a model that matches key empirical features of real option data. Our Monte Carlo results show that the accuracy of the estimator depends strongly on the time of the trading day. In particular, the precision of the estimation is lower for estimating the value of the periodic function at the earlier part of the trading day because the signal to noise ratio is weaker at that time. Relative to a standard return-based estimator of the intraday volatility pattern, the option-based one (constructed over the same time window as the return-based one) offers nontrivial efficiency gains, particularly towards the end of the trading day. Moreover, since option- and return-based estimates of the intraday volatility pattern are asymptotically uncorrelated, one can combine the two estimates to increase further precision.

We apply our estimation procedure to S&P 500 index options over the period 2018-2020. We use intraday option observations on Fridays with expiration on the same day and on the following trading day (typically Monday). We estimate the intraday volatility pattern on a yearly basis. Our results reveal variation in the ratio of volatility at the beginning and at the end of the trading day over the sample period.

The rest of the paper is organized as follows. In Section 2, we introduce our setting and the option observation scheme. In Section 3, we present our option-based estimate of the intraday periodic component of volatility and analyze its asymptotic properties. Section 4 contains a Monte Carlo study and Section 5 our empirical application. Section 6 concludes. Additional estimation results as well as the technical assumptions and the proofs are given in Section 7.

2 Setting and Option Observation Scheme

The asset price process is denoted with X and the logarithm of it with x. The price process is defined on the sample space Ω, with the associated σ-algebra $\mathcal{F}$, and $(\mathcal{F}_t)_{t\in\mathbb{R}_+}$ being the filtration.

We will consider two probability measures, one being the true (statistical) one, denoted with $\mathbb{P}$, and the other one being the risk-neutral one, denoted with $\mathbb{Q}$. The latter, under the weak condition of arbitrage-free asset prices, is locally equivalent to the true one. The significance of $\mathbb{Q}$ stems from the fact that the payoff process of any asset, discounted at the risk-free rate, is a local martingale under $\mathbb{Q}$. We will use this result to connect the value of derivatives written on the asset with its volatility. More specifically, the dynamics of x under $\mathbb{Q}$ is given by

$$dx_t = \alpha_t dt + \sqrt{\eta_{t/\kappa - \lfloor t/\kappa \rfloor}}\sigma_t dW_t + \int_{\mathbb{R}} x\mu(dt, dx), \tag{1}$$

where W is a $\mathbb{Q}$ Brownian motion and μ is an integer-valued random measure on $\mathbb{R}_+ \times \mathbb{R}$ with $\mathbb{Q}$ jump compensator $dt \otimes \eta_{t/\kappa - \lfloor t/\kappa \rfloor} \nu_t(dx)$, for some predictable measure ν_t satisfying $\int_{\mathbb{R}} |x| \nu_t(dx) < \infty$. Finally, $\eta : [0, 1] \to \mathbb{R}_+$ is a *deterministic* function capturing the intraday periodicity in volatility. The length of the periodic cycle is an interval from market close on one day till market close on the next trading day (one business day). The length of that period is denoted with κ. Our interest in this paper is the study of the function η from short-dated option observations.

We note that local equivalence of $\mathbb{P}$ and $\mathbb{Q}$ implies that x obeys the same dynamics under $\mathbb{P}$ but with a different drift coefficient $\alpha_t^{\mathbb{P}}$ and a different jump compensator measure $\nu_t^{\mathbb{P}}(dx)$. The diffusion coefficient σ_t is the same under the two probability measures. Importantly, since η_t is deterministic function, it does not change when switching from $\mathbb{Q}$ to $\mathbb{P}$.

Remark 1. *In the specification in (1), we assumed that the periodic component of the diffusive variance is the same as that of the jump intensity. This seems a natural assumption and it is implicitly imposed by earlier studies that do not separate diffusive variance from jumps. If however, one is interested only in the periodic component of diffusive variance, without making assumptions about the periodicity of jumps, then the analysis that follows should be modified by making use of jump-robust estimates of volatility from options data like the ones proposed in Todorov (2019). We present such results in Section 7.1. They provide support for the above assumption that equates the periodicity in diffusive variance with that in the jump intensity.*

We turn next to our option observation scheme. We denote with $O_{t,T}(K)$ the price at time t of a European-style out-of-the-money option price written on the asset and expiring at time $t + T$. We recall that $O_{t,T}(K)$ is the minimum of the put and call option prices with strike K. The option prices corresponding to the pair (t, T) are observed on the following discrete strike grid:

$$K_{t,T}(1) < ... < K_{t,T}(N_{t,T}), \;\; N_{t,T} \in \mathbb{N}_+. \tag{2}$$

Option prices are observed with error, i.e., we observe

$$\widehat{O}_{t,T}(K_{t,T}(j)) = O_{t,T}(K_{t,T}(j)) + \epsilon_{t,T}(j), \tag{3}$$

where the errors $\epsilon_{t,T}(j)$ are defined on a space $\Omega^{(1)} = \mathbb{R}^{\mathbb{R}} \times \mathbb{R}^{\mathbb{R}}$ which is equipped with the product Borel σ-field $\mathcal{F}^{(1)}$, and transition probability $\mathbb{P}^{(1)}(\omega^{(0)}, d\omega^{(1)})$ from the probability space $\Omega^{(0)}$, on which X is defined, to $\Omega^{(1)}$. We further define,

$$\Omega \,=\, \Omega^{(0)} \times \Omega^{(1)}, \quad \mathcal{F} \,=\, \mathcal{F}^{(0)} \times \mathcal{F}^{(1)},$$

and

$$\mathbb{P}(d\omega^{(0)}, d\omega^{(1)}) \,=\, \mathbb{P}^{(0)}(d\omega^{(0)})\, \mathbb{P}^{(1)}(\omega^{(0)}, d\omega^{(1)})\,.$$

We assume that we observe the options on the following equidistant time grid:

$$t_0 = 0 < t_1 < t_2 < ... < t_n = \left(\left\lfloor \frac{\kappa}{\Delta} \right\rfloor - 3 \right) \Delta, \tag{4}$$

with $t_i - t_{i-1} = \Delta$, for some $0 < \Delta < \kappa$. This corresponds to intraday sampling of option prices like in our application. At each sampling time t_i, we will have observations of options with two tenors, T_i^0 and T_i^1. The shorter tenor will be $T_i^0 = \kappa - t_i$ and the longer one will be $T_i^1 = T_i^0 + \kappa$. That is, the shorter tenor will correspond to zero-day options expiring on the same trading day and the longer tenor to options expiring on the next trading day.

To simplify notation, we will use the following shorthand notation henceforth: $N_{i,l} = N_{t_i,T_i^l}$, $K_{i,l}(j) = K_{t_i,T_i^l}(j)$, $\epsilon_{i,l}(j) = \epsilon_{t_i,T_i^l}(j)$ and $\widehat{O}_{i,l}(j) = \widehat{O}_{t_i,T_i^l}(K_{t_i,T_i^l}(j))$, for $l = 0, 1$ and $j = 1, ..., N_{t_i,T_i^l}$.

Remark 2. *In the specification of x in (1), η is assumed to be a deterministic function. However, as will become clear from the analysis below, we only need that η is $\mathcal{F}_0$-adapted for the estimator that we propose. For notational simplicity, we will present our results for η deterministic.*

3 Estimation of the Periodic Component of Volatility

Our strategy for recovering the periodic component of volatility is to form measures of conditional risk-neutral expectation of future return variation over the two tenors of the available options. These conditional expectations will depend both on the periodic (and deterministic) volatility component as well as on its stochastic component. By taking advantage of the two tenors and the fact that they are both short, we can suitably cancel out the stochastic components of the conditional expectations of future return variation and identify the periodic volatility component.

We now provide the details about our estimation strategy. Using the formula for computing the VIX index, see e.g., Britten-Jones and Neuberger (2000) and Carr and Wu (2009), we have

$$QV_{t,T} \equiv \mathbb{E}_t^{\mathbb{Q}} \left(\int_t^{t+T} \eta_{s/\kappa - \lfloor s/\kappa \rfloor} \left(\sigma_s^2 + 2 \int_{\mathbb{R}} (e^x - 1 - x) \nu_s(dx) \right) ds \right) = 2 \int_0^{\infty} \frac{O_{t,T}(K)}{K^2} dK. \tag{5}$$

We note that the integral in $QV_{t,T}$ is not exactly the quadratic variation of the log-price, with the deviation from the latter being due to the price jumps. This difference, however, will play no role in our analysis henceforth.

Using the available options, a Riemann sum approximation of the integral in (5) leads to the following feasible counterpart of the risk-neutral conditional expectation of the quadratic variation:

$$\widehat{QV}_{t,T} = 2\sum_{j=2}^{N_{t,T}} \frac{\widehat{O}_{t,T}(K_{t,T}(j-1))}{K_{t,T}^2(j-1)}(K_{t,T}(j) - K_{t,T}(j-1)). \tag{6}$$

With the help of $\widehat{QV}_{t,T}$, we can construct estimates of the function η.[2] Recall that we have observations of options at the discrete times t_i, for $i = 0, 1, ..., n$. Then, we set

$$\widehat{QV}_\phi^{(0)} = \widehat{QV}_{t_i,T_i^0} \text{ and } \widehat{QV}_\phi^{(1)} = \widehat{QV}_{t_i,T_i^1}, \text{ for } i = \left\lfloor \frac{\phi\kappa}{\Delta} \right\rfloor \text{ and } \phi \in [0, 1). \tag{7}$$

With this notation, we introduce

$$\widehat{\eta}_\phi = \frac{\widehat{QV}_\phi^{(0)}}{\widehat{QV}_\phi^{(1)} - \widehat{QV}_\phi^{(0)}}, \ \phi \in [0, 1). \tag{8}$$

We will show that $\widehat{\eta}_\phi$ is an estimator of $\int_\phi^1 \eta_s ds / \int_0^1 \eta_s ds$ (note that η is uniquely identified up to a constant only). From here, we can also define

$$\widehat{\eta}_{\phi_1,\phi_2} = \widehat{\eta}_{\phi_2} - \widehat{\eta}_{\phi_1}, \ 0 \le \phi_1 < \phi_2 < 1, \tag{9}$$

which is an estimator of $\int_{\phi_1}^{\phi_2} \eta_s ds / \int_0^1 \eta_s ds$.[3] In what follows, we will be interested in the asymptotic properties of $\widehat{\eta}_\phi$ and $\widehat{\eta}_{\phi_1,\phi_2}$. The latter, in particular, can be used for studying the intraday volatility pattern we are after.

For this, we will first derive a CLT result for $\widehat{QV}_\phi^{(0)}$ and $\widehat{QV}_\phi^{(1)}$, for some fixed $\phi \in [0, 1)$. The convergence in distribution result will hold $\mathcal{F}^{(0)}$-conditionally. This is denoted by $\xrightarrow{\mathcal{L}|\mathcal{F}^{(0)}}$ and formally means convergence in probability of the conditional probability laws when the latter are considered as random variables taking values in the space of probability measures equipped with the weak topology, see e.g., VIII.5.26 of Jacod and Shiryaev (2003).

[2] $\widehat{QV}_{t,T}$, with T corresponding to same day expiration and next day expiration that we work with here, are used by CBOE for calculating the 1-day VIX.

[3] Even if the intraday pattern on the two days differ, we can still use $\widehat{\eta}_{\phi_1,\phi_2}$ as an estimator of the intraday periodic component of volatility on the current day. More specifically, suppose that the periodic component of volatility on the current day is given by $\eta^{(0)}$ and by $\eta^{(1)}$ on the following day. In that case, it is easy to show that $\widehat{\eta}_\phi$ is a consistent estimate of $\int_\phi^1 \eta_s^{(0)} ds / \int_0^1 \eta_s^{(1)} ds$. Thus, by varying ϕ, we can learn about the function $\eta^{(0)}$ (but not about $\eta^{(1)}$), which is identified up to a constant only.

For stating the next theorem, we introduce the following additional notation

$$\widetilde{\Phi}(k) = f(k) + |k|\Phi(-|k|), \quad k \in \mathbb{R}, \tag{10}$$

where f and Φ are the pdf and cdf, respectively, of a standard normal random variable. We also use the shorthand notation $\underline{K} = \max_{i=1,\dots,n,\, l=0,1} K_{i,l}(1)$ and $\overline{K} = \min_{i=1,\dots,n,\, l=0,1} K_{i,l}(N_{i,l})$. We note that $\underline{K}$ and $\overline{K}$ will typically correspond to the minimum and maximum available strike, respectively, at the last observation time t_n. Finally, in the theorem below, δ denotes a reference "average" log-strike gap, formally defined in assumption A3.

Theorem 1. *Suppose assumptions A1-A4 hold and fix $\phi \in [0,1)$. Let $\kappa \downarrow 0$ and $\delta \asymp \kappa^{\alpha}$, $\underline{K} \asymp \kappa^{\beta}$, $\overline{K} \asymp \kappa^{-\gamma}$, for $\alpha > \frac{1}{2}$ and $\beta, \gamma > \frac{\alpha}{4} - \frac{1}{8}$. In addition, let $\frac{\Delta}{\sqrt{\delta}\kappa^{3/4}} \to 0$. We have*

$$\frac{1}{\sqrt{\delta}\kappa^{3/4}} \begin{pmatrix} \widehat{QV}_{\phi}^{(0)} - QV_{\phi\kappa,(1-\phi)\kappa} \\ \widehat{QV}_{\phi}^{(1)} - QV_{\phi\kappa,(2-\phi)\kappa} \end{pmatrix} \xrightarrow{\mathcal{L}|\mathcal{F}^{(0)}} \begin{pmatrix} Z_{\phi,0} \\ Z_{\phi,1} \end{pmatrix}, \tag{11}$$

where $\mathcal{F}^{(0)}$-conditionally $(Z_{\phi,0},\, Z_{\phi,1})$ is a centered Gaussian vector with $\mathcal{F}^{(0)}$-conditional variance given by $\Sigma_{\phi} = \mathrm{diag}(\Sigma_{\phi,0},\, \Sigma_{\phi,1})$, with

$$\Sigma_{\phi,l} = \left(\int_{\phi}^{1} \eta_s ds + 1_{\{l=1\}} \int_{0}^{1} \eta_s ds\right)^{3/2} \sigma_0^3 \psi_{0,l}(0)\zeta_{0,l}^2(0) \int_{\mathbb{R}} \widetilde{\Phi}^2(k)dk, \;\; l = 0, 1, \tag{12}$$

where the functions $\psi_{t,l}$ and $\zeta_{t,l}$, for $l = 0, 1$, appear in assumption A4.

We make several observations about the above CLT result. First, the rate of convergence of the risk-neutral quadratic measures is determined from the options with strikes in the vicinity of the current spot price. The reason for this is that, these options dominate asymptotically the rest of the options with strikes away from the current spot price. We refer to Lemma 1 for a formal statement of this. In turn, the asymptotic behavior of the near-the-money options is dominated by the diffusive component of the underlying asset price. Thus, in spite of the fact that $\widehat{QV}_{t,T}$ is a measure of total return variation that includes jumps, its asymptotic behavior for T small is governed by the diffusive component of the underlying price. Second, the rate of convergence in the CLT is determined by the mesh of the log-strike grid δ and the bound on the time-to-maturity of the options κ. Third, the asymptotics here is of joint type as we require δ and κ to go to zero simultaneously and also $\underline{K} \to 0$ and $\overline{K} \to \infty$.

In the statement of the theorem, we impose various rate conditions that ensure that biases that arise in the estimation are of higher asymptotic order. In particular, the rate condition for $\underline{K}$

and $\overline{K}$ guarantees that the bias due to the truncation of the two tails in the integration in (5) is negligible. This bias is given by

$$2\int_0^{K_{i,l}(1)} \frac{O_{i,l}(K)}{K^2}dK + 2\int_{K_{i,l}(N_{i,l})}^{\infty} \frac{O_{i,l}(K)}{K^2}dK, \quad i = \left\lfloor \frac{\phi\kappa}{\Delta} \right\rfloor, \quad l = 0, 1. \tag{13}$$

How big the above bias is depends naturally on how fat are the tails of the return distribution. This, in turn, is related to the tail behavior of the jumps because in our case $\kappa \downarrow 0$. Assuming that the law of the big jumps of x belongs to the Fréchet maximum domain of attraction, see e.g., Bollerslev and Todorov (2014), with left and right tail decay parameters of $\alpha_{\pm} > 0$, the leading term of the above bias is given by

$$\frac{2}{\alpha_- - 1}\frac{O_{i,l}(K_{i,l}(1))}{K_{i,l}(1)} + \frac{2}{\alpha_+ + 1}\frac{O_{i,l}(K_{i,l}(N_{i,l}))}{K_{i,l}(N_{i,l})}. \tag{14}$$

In practice, $O_{i,l}(K_{i,l}(1))$ and $O_{i,l}(K_{i,l}(N_{i,l}))$ are determined by the minimum bid and ask quotes on the exchange (our option observation is the mid-quote) and hence typically do not vary over time. Given that $\kappa \downarrow 0$, $K_{i,l}(1)$ and $K_{i,l}(N_{i,l})$ are close to the current stock price $X_{\phi\kappa}$. Thus, in practice, the downward bias due to truncation of the limits of integration does not change by much as ϕ varies. On the other hand, the estimands of $\{\widehat{QV}_{\phi}^{(l)}\}_{l=0,1}$ shrink as ϕ converges to one. As a result, in relative terms this bias naturally becomes more prominent as ϕ increases. While this is problematic for the estimation of $QV_{\phi}^{(0)}$ when ϕ is close to one, note that our interest is in the estimand of $\widehat{\eta}_{\phi_1,\phi_2}$ during the trading day. Since the truncation biases in $\widehat{\eta}_{\phi_1}$ and $\widehat{\eta}_{\phi_2}$ are approximately the same, as argued above, they will cancel out in $\widehat{\eta}_{\phi_1,\phi_2} = \widehat{\eta}_{\phi_2} - \widehat{\eta}_{\phi_1}$. Thus, from a practical point of view, the truncation bias should not be of concern here for our purposes. We will confirm this in the Monte Carlo.

Next, the requirement $\delta \asymp \kappa^{\alpha}$ with $\alpha > 1/2$ guarantees that error due to the Riemann sum approximation of the integral in (5) is of higher order. If this condition does not hold, then the change of the option price as the strike moves on the strike grid in the vicinity of the current stock price will be too big, which in turn will cause the Riemann sum approximation error to be big. From a practical point of view, the strike grid is fixed by the exchange,[4] so the above rate condition involving δ and κ puts a limit on how short the tenor of the options can be for our asymptotics to work well. This will be discussed later on in the Monte Carlo analysis.

When $\delta/\sqrt{\kappa} \to 0$, then the Riemann sum approximation error is always dominated by the observation error in the options which drive the CLT result in Theorem 1. Due to the leading role in the estimation played by the options with strikes in vicinity of the current stock price, the

[4]For example, for the S&P 500 index options used in our empirical analysis it is set to 5.

discretization error around-the-money dominates the remaining part of this error. Since around-the-money options are approximated by the Black-Scholes formula (see Lemma 1), out-of-the-money puts and calls with strikes that are equal distance from the spot price are approximately the same. Hence, there will be cancelation in the discretization error around the money. Furthermore, one can perform linear interpolation of the observed option prices on a finer strike grid in Black-Scholes implied volatility space and form the Riemann sum from the interpolated prices. This will reduce the discretization error and has been often done in empirical work, see e.g., Carr and Wu (2009).

Finally, the requirement $\frac{\Delta}{\sqrt{\delta}\kappa^{3/4}} \to 0$ is due to the fact that the option observations are on a discrete grid while our interest is estimation at a fixed point in time (which is not necessarily on the observation time grid). If the centering of $\widehat{QV}_{\phi}^{(0)}$ and $\widehat{QV}_{\phi}^{(1)}$ is with their limits at the observation time, then this condition will not be necessary.

Remark 3. *The CLT result of the theorem is derived under the assumption that the ratio of the option observation error to the true (latent) option price is $O_p(1)$, see assumption A4. Empirically, the ratio of option bid-ask spread to the mid-quote, which can be viewed as a proxy for the relative option observation error, is a small number, see e.g., Andersen et al. (2015a). We can generalize the result of the above theorem by allowing for the relative option pricing error to shrink to zero. The result of Theorem 1 can be extended to cover such a situation, with the rate of decay of the option observation error showing up in the rate of convergence of the estimator.*

Remark 4. *Assumption A4 in the Appendix assumes that the observation errors are $\mathcal{F}$-conditionally independent across strikes and over time. This requirement can be relaxed to allow for weak time-series and spatial dependence. Andersen et al. (2021) document only very mild spatial dependence in short-dated SPX options that we are going to use in the empirical application. For that reason, we will not consider an extension of Theorem 1 that allows for weak $\mathcal{F}$-conditional dependence in the observation errors.*

The limit quantities $QV_{\phi\kappa,(1-\phi)\kappa}$ and $QV_{\phi\kappa,(2-\phi)\kappa}$ can be used to estimate the periodic component of volatility by taking advantage of the fact that κ is small and that the stochastic component of the diffusive volatility and of the jump intensity is smooth in expectation by our assumption A1. We note in this regard that we do not require an assumption regarding the smoothness of the periodic component η. The next theorem presents the formal result.

Theorem 2. *Suppose assumptions A1-A2 hold and fix $\phi \in [0, 1)$. We have*

$$\frac{QV_{\phi\kappa,(1-\phi)\kappa}}{QV_{\phi\kappa,(2-\phi)\kappa} - QV_{\phi\kappa,(1-\phi)\kappa}} - \frac{\int_{\phi}^{1} \eta_s ds}{\int_{0}^{1} \eta_s ds} = O_p(\kappa). \tag{15}$$

The bound on the error in the above theorem is sharp and is directly linked to the assumed degree of smoothness of the stochastic component of diffusive volatility and jump intensity given in assumption A1. This assumption is satisfied when diffusive volatility and jump intensity are modeled via Itô semimartingales, which is the case for most asset pricing models used in applied work.

By combining the results of the above two theorems, we can arrive at a feasible estimate of tail integrals of the periodic component of volatility. The result is stated in the following corollary.

Corollary 1. *Suppose the conditions in Theorem 1 hold. We then have*

$$\frac{\kappa^{1/4}}{\sqrt{\delta}}\left(\widehat{\eta}_\phi - \frac{\int_\phi^1 \eta_s ds}{\int_0^1 \eta_s ds}\right) \xrightarrow{\mathcal{L}|\mathcal{F}^{(0)}} \sqrt{Avar(\widehat{\eta}_\phi)}Z, \tag{16}$$

where Z is a standard normal random variable defined on an extension of the original probability space and independent from $\mathcal{F}$ and

$$Avar(\widehat{\eta}_\phi) = \frac{\left(\int_\phi^1 \eta_s ds + \int_0^1 \eta_s ds\right)^2}{v_0^2\left(\int_0^1 \eta_s ds\right)^4}\Sigma_{\phi,0} + \frac{\left(\int_\phi^1 \eta_s ds\right)^2}{v_0^2\left(\int_0^1 \eta_s ds\right)^4}\Sigma_{\phi,1}, \tag{17}$$

with v_0 given by

$$v_0 = \sigma_0^2 + 2\int_{\mathbb{R}}(e^x - 1 - x)\nu_0(dx). \tag{18}$$

In addition, $\widehat{\eta}_{\phi_1}$ and $\widehat{\eta}_{\phi_2}$ are $\mathcal{F}^{(0)}$-conditionally asymptotically independent for $\phi_1 \neq \phi_2$.

The $\mathcal{F}^{(0)}$-conditional asymptotic variance of $\widehat{\eta}_{\phi_1,\phi_2}$ is given by $\text{Avar}(\widehat{\eta}_{\phi_1}) + \text{Avar}(\widehat{\eta}_{\phi_2})$. We note also that in the above Corollary, we do not need any additional requirement for the option observation scheme than what is already assumed in Theorem 1.

Given the limit result in Corollary 1, we can analyze the precision in the estimation as a function of time of day, i.e., as a function of ϕ. This is easiest to do in the case when $\psi_{0,0}(0) = \psi_{0,1}(0)$ and $\zeta_{0,0}(0) = \zeta_{0,1}(0)$, where the functions $\{\psi_{t,l}\}_{l=0,1}$ and $\{\zeta_{t,l}\}_{l=0,1}$ are given in assumption A4. These quantities are related to the denseness of the strike grid and the variance of the option observation error for the two tenors. With this simplifying assumption, we have

$$\text{Avar}(\widehat{\eta}_\phi) \propto \left(\int_\phi^1 \eta_s ds\right)^{3/2}\left(\int_\phi^1 \eta_s ds + \int_0^1 \eta_s ds\right)^2 + \left(\int_\phi^1 \eta_s ds\right)^2\left(\int_\phi^1 \eta_s ds + \int_0^1 \eta_s ds\right)^{3/2}, \tag{19}$$

with $\propto$ above means that $\text{Avar}(\widehat{\eta}_\phi)$ equals the right-hand-side of (19) times a random variable that does not depend on ϕ. It is easy to see now that the precision in the estimation increases as ϕ approaches one. The reason for this is as follows. $\int_\phi^1 \eta_s ds$ increases when ϕ decreases, i.e., when we look at earlier parts of the trading day. Since option observation errors are proportional to option prices, this automatically translates in larger noise (in absolute terms) in $\widehat{QV}_{\phi\kappa,(1-\phi)\kappa}$ and $\widehat{QV}_{\phi\kappa,(2-\phi)\kappa}$ for lower values of ϕ. This can explain the dependence of $\mathrm{Avar}(\widehat{\eta}_\phi)$ on ϕ. This strong dependence of the precision of the estimation on the time of day will carry over to the situation where one uses longer-tenor options than the ones used here to recover η. That is, if one attempts estimation of η on the basis of options $\widehat{QV}_{\phi\kappa,(k-\phi)\kappa}$, for some $k > 1$, then the precision of such estimation would drop significantly relative to our estimator based on zero- and one-day tenor options.

The same observations naturally apply to the estimator $\widehat{\eta}_{\phi_1,\phi_2}$. The differencing reduces the signal (i.e., $\int_{\phi_1}^{\phi_2} \eta_s ds$ is much smaller than $\int_{\phi_1} \eta_s ds$ when ϕ_2 is close to ϕ_1) while the noise (i.e., the estimation error) increases. This implies that estimation of $\int_{\phi_1}^{\phi_2} \eta_s ds$ is significantly harder than estimation of $\int_{\phi_1}^{1} \eta_s ds$ and that the precision in estimating $\int_{\phi_1}^{\phi_2} \eta_s ds$ increases as $\phi_1, \phi_2 \to 1$.

Finally, although feasible estimates of $\mathrm{Avar}(\widehat{\eta}_\phi)$ are theoretically possible, see e.g., Todorov (2019), we will not provide such here as we conjecture that reliable fully nonparametric estimation of the asymptotic variance will be difficult given the very short tenor of the options used in the analysis (which results in nontrivial changes in the true option prices around-the-money).

4 Monte Carlo Study

In this section, we evaluate the performance of the option-based estimator of the periodic volatility component on simulated data.

4.1 Setup

We use the following model for the underlying asset dynamics, under the risk-neutral probability, to generate the true option prices:

$$\frac{dX_t}{X_{t-}} = \sqrt{V_t} dW_t + \int_{\mathbb{R}} (e^x - 1)\, \mu(dt, dx), \tag{20}$$

$$dV_t = \kappa_v(\theta_v - V_t)dt + \sigma_v \sqrt{V_t} dB_t, \tag{21}$$

where W_t and B_t are $\mathbb{Q}$ Brownian motions with $\mathrm{corr}(dW_t, dB_t) = \rho dt$, and μ is an integer-valued random measure with $\mathbb{Q}$ compensator $dt \otimes \nu_t(dx)$, for ν_t given by

$$\nu_t(dx) = V_t \times \nu^{ts}(x)dx,\ \nu^{ts}(x) = c_- \frac{e^{-\lambda_-|x|}}{|x|^{1+\alpha}} 1_{\{x<0\}} + c_+ \frac{e^{-\lambda_+|x|}}{|x|^{1+\alpha}} 1_{\{x>0\}}. \tag{22}$$

In the above specification for X, the stochastic variance is modeled as a square-root diffusion process like in the popular model of Heston (1993). The jump intensity is affine in the level of diffusive variance like in the stochastic volatility model of Duffie et al. (2000) and subsequent empirical option pricing work. Our jump specification is a time-changed tempered stable process, see Carr et al. (2003), with the time-change being the integrated diffusive variance. We allow for different parameters to control the negative and positive jumps. Throughout, we set $\lambda_- = 100$ and $\lambda_+ = 200$. This generates tail decays in deep out-of-the-money puts and calls with zero and one day to expiration that are similar to those observed in our empirical application. We set $c_\pm$ according to

$$c_- = 0.9 \times \frac{\lambda_-^{2-\alpha}}{\Gamma(2-\alpha)} \text{ and } c_+ = 0.1 \times \frac{\lambda_+^{2-\alpha}}{\Gamma(2-\alpha)},$$

which implies that risk-neutral spot jump variation is equal to spot diffusive variance, and further that 90% of the jump variation is due to negative jumps. This separation of the risk-neutral variation into diffusive and one due to positive and negative jumps is similar to that implied from parametric models fitted to observed S&P 500 index options, see e.g., Andersen et al. (2015b). Finally, we set the parameter α, which governs the behavior of the small jumps, to 1.8. This implies presence of a lot of smaller-sized jumps.[5]

In our model in the Monte Carlo, the periodic function is the identity. This allows us to obtain option prices in semi-closed form, which will not be the case otherwise.[6] Our goal in the Monte Carlo is to investigate the effect from the mean reversion in the stochastic component of volatility, the discreteness and finite range of the strike grids and the option observation error on the precision in recovering the intraday periodic component of volatility. For this, a Monte Carlo setup with η being the identity function should suffice.

We consider two parameter settings for the diffusive variance dynamics. In both of them, we set the mean of the variance to $\theta_v = 0.02$ and the correlation between the two Brownian motions to $\rho = -0.9$. These parameters match roughly estimates from prior empirical work for the risk-neutral mean of variance and the leverage effect. In the first of our two specifications, case S, we set κ_v so that the half-life of a shock to variance is one month. In the second specification, case F, we increase the speed of mean reversion by setting κ_v so that the half-life of a shock to variance is only one week. In both cases, we set the volatility of volatility parameter σ_v so that the coefficient of variation of V (given by $\sigma_v/\sqrt{2\kappa_v\theta_v}$) is equal approximately to 0.35. The parameter values for the two cases are given in Table 1.

We turn next to the option observation scheme. Observed options are given by

$$\widehat{O}_{t,T}(k_{t,T}(j)) = O_{t,T}(k_{t,T}(j))(1 + 0.015 \times z_{t,T}(j)), \; j = 1, ..., N_{t,T}, \tag{23}$$

[5]The parameter α should be below 2 and higher values of α means higher rate of explosion of ν^{ts} around zero.

[6]We are grateful to Nicola Fusari for providing the option pricing codes used in the Monte Carlo section.

Table 1: **Parameter Setting for the Monte Carlo**

Case	Variance Parameters				Jump Parameters				
	θ_v	κ_v	σ_v	ρ	α	λ_-	λ_+	c_-	c_+
S	0.02	8.3	0.2	-0.9	1.8	100	200	0.4924	0.0629
F	0.02	34.9	0.4	-0.9	1.8	100	200	0.4924	0.0629

where $\{z_{t,T}(j)\}_{j=1}^{N_{t,T}}$ are sequences of i.i.d. standard normal variables which are independent of each other. The size of the observation error is calibrated to match roughly bid-ask spreads of index option data around the money. The initial level of the stock price at the start of the day is set to 3500. For each pair (t, T), the strikes are multiples of 5. The strikes below and above the current price are extended in both directions by increments of 5 until the true out-of-the-money option price falls below 0.075. This specification of the strike grid mimics that of available of S&P 500 index options. The starting value of the diffusive variance at the beginning of the day is set to 25-th, 50-th or 75-th quantile of its marginal distribution. Option prices are observed at 77 equidistant times in a trading day. This corresponds to sampling at a five-minute frequency over the period 9.35-15.55 EST in a trading day. Note that the option trading day at CBOE, where S&P 500 index options are traded, lasts over the period $9.30 - 16.15$ EST. Therefore, in our case $\Delta = 1/(252 \times 82)$. Finally, the time to maturities T_1^0 and T_1^1 are equal to $81/(252 \times 82)$ and $1/252 + 81/(252 \times 82)$, respectively.

4.2 Precision of the Option-based Estimator

Before presenting the results from the Monte Carlo, we assess the effect of the Riemann sum discretization error and the error due to truncation of the integral in (5) on the estimator. For this purposes, we switch off the observation error and consider the last increment during the day, 15.50-15.55 EST where the effect of these errors should be largest. We use case S for this illustration and set the starting value of volatility at the 25-th quantile of the unconditional distribution of V_t. The value of the underlying stock price is drawn uniformly from an equidistant grid of points covering the interval $3500.5 - 3505$ at increments of 0.5 (recall that the gaps between strikes in our setup is 5). For this setting, the number of out-of-the-money options used in the estimation is only 8. We first assess the size of the truncation error. For $\widehat{\eta}_\phi$, the relative size of this error is approximately 2%. Due to the partial cancelation of this error that we discussed in the previous section, its relative size for $\widehat{\eta}_{\phi_1,\phi_2}$ gets reduced significantly to 0.5%. We next evaluate the size of the Riemann sum discretization error. For this purpose, we compare $\widehat{\eta}_\phi$ and $\widehat{\eta}_{\phi_1,\phi_2}$ using the coarse strike grid with increments of 5, described above, with a finer strike grid with increments of only 0.1. We find that the relative discretization error for $\widehat{\eta}_\phi$ is around 4% and only 0.5% for $\widehat{\eta}_{\phi_1,\phi_2}$. Overall, these results show that higher-order biases due to the Riemann sum discretization error and the truncation error are small in relative terms for the estimator $\widehat{\eta}_{\phi_1,\phi_2}$ even when one looks at the end of the trading day.

We proceed with the general Monte Carlo results which are summarized in Figures 2 and 3. For both parameter settings and for all starting values of volatility, we can notice a strong monotone increase in the precision of the estimation, with the noisiest estimation being for the value of the periodic volatility function at the start of the trading day. This is consistent with the dependence of the asymptotic variance of $\widehat{\eta}_\phi$ on ϕ, see equation (19) above.

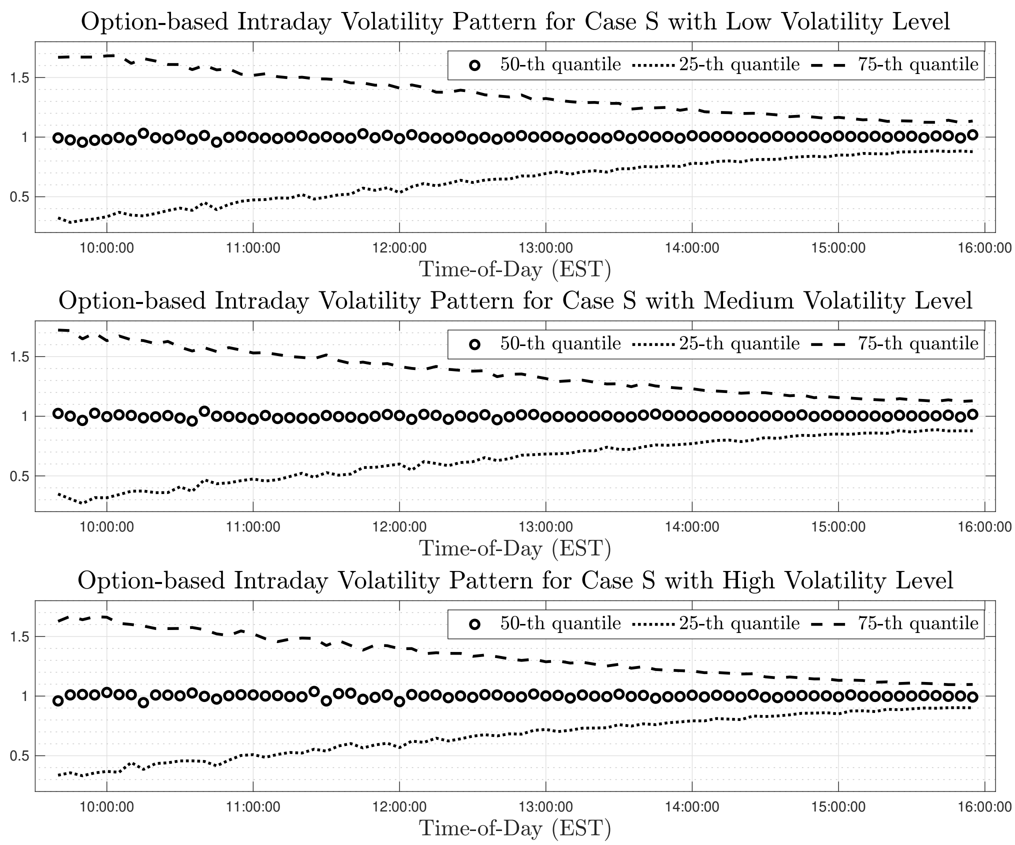

Figure 2: **Monte Carlo Results for Simulation Scenario S**. For each time of day, we report 25-th, 50-th and 75-th quantile of the estimate of $\widehat{\eta}_{\phi_1,\phi_2}$, for ϕ_1 and ϕ_2 corresponding to consecutive observations on a 5-minute grid covering the time interval $9.35 - 15.55$ EST. The estimates are standardized by dividing by their average value across the times-of-day. The number of Monte Carlo replications is 3000.

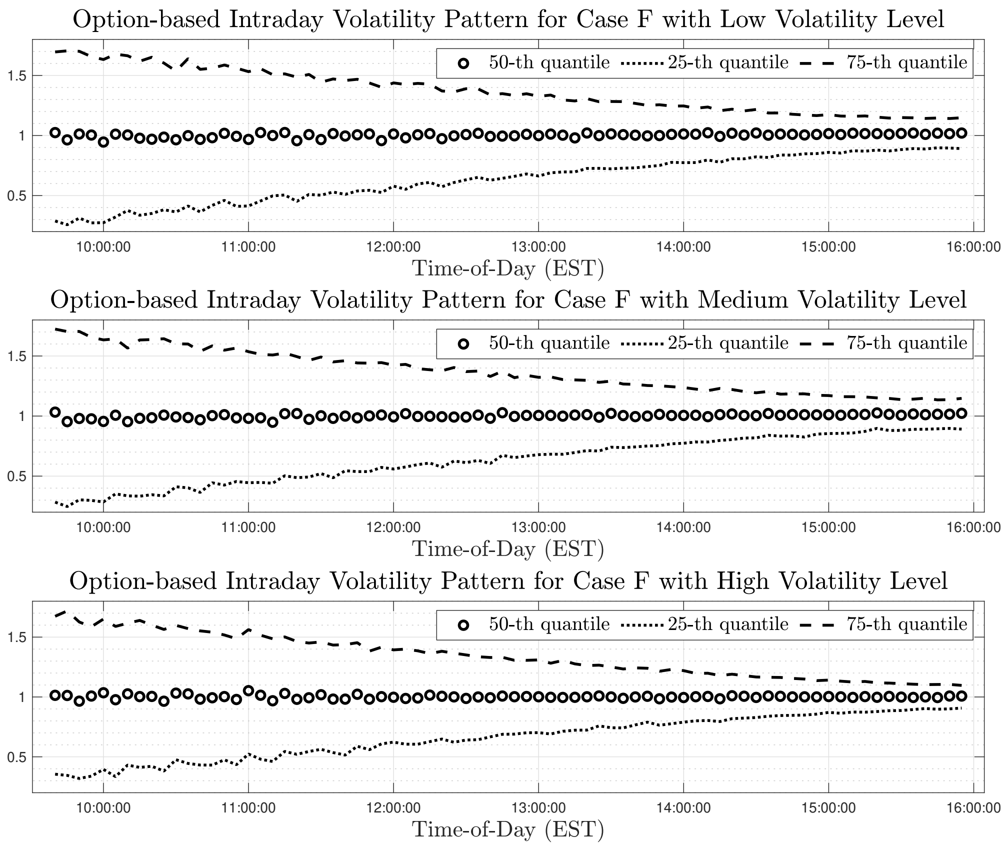

Figure 3: **Monte Carlo Results for Simulation Scenario F**. For each time of day, we report 25-th, 50-th and 75-th quantile of the estimate of $\widehat{\eta}_{\phi_1,\phi_2}$, for ϕ_1 and ϕ_2 corresponding to consecutive observations on a 5-minute grid covering the time interval $9.35 - 15.55$ EST. The estimates are standardized by dividing by their average value across the times-of-day. The number of Monte Carlo replications is 3000.

Another observation from the reported Monte Carlo results is that the precision of the estimation appears slightly higher for higher values of the volatility. This difference is nevertheless very small. The explanation for that effect is that when volatility is higher, we have more option observations on average. Thus, in this case the option observation error can be more effectively "diversified away" in the option portfolios $\widehat{QV}_{\phi\kappa,(1-\phi)\kappa}$ and $\widehat{QV}_{\phi\kappa,(2-\phi)\kappa}$. That said, we note that what matters for the limiting distribution is not the total number of options per tenor but rather the number of those around the money. For this reason, the dependence of the estimation precision on the level of volatility is not very strong.

Finally, comparing the results in the two figures, we can detect little differences in the estimation in the two parameter settings. In particular, in both cases the medians of the estimates are not very different from their true values (recall in the Monte Carlo η is the identity function). This suggests that the effect from mean-reversion in the stochastic component of volatility on the recovery of η is negligible. This is, of course, due to the very short tenor of the options used in the estimation.

Overall the reported Monte Carlo results show that the intraday periodic component of volatility can be reliably estimated from short-dated options. While estimation using a single day of data is considerably noisy, pooling option data across several trading days should significantly improve the precision.

4.3 Comparison with a Return-based Estimator

We next compare the precision of the option-based estimator of the periodic function η with a nonparametric one constructed from high-frequency data.We note that the asymptotic behavior of option- and return-based estimators is very different. When one uses options, then this is equivalent to having direct observations of expectations of future volatility over different short horizons contaminated with measurement error. Thus, the option observation error governs the limiting behavior of the option-based estimator of η. On the other hand, when one uses high-frequency returns, we do not have direct observations of expectations of future volatility over different horizons. Instead, we need to resort to long-span asymptotics and a Law of Large Numbers to disentangle the periodic component of volatility from its stationary part. As a result, the limiting distribution of a return-based estimator of η is determined by the empirical process error associated with the latent stationary component of volatility, see Andersen et al. (2023). This is in sharp contrast to the option-based estimator which does not require any stationarity assumption for the volatility.

This very different asymptotic behavior of the option- and return-based estimators of η means that they are best compared in a Monte Carlo experiment. This is what we do here. Towards this end, denote the increment of the log-price with $\Delta_{j,i}^n x = x_{(j-1)\kappa+i\Delta} - x_{(j-1)\kappa+(i-1)\Delta}$. The return-based estimator of intraday periodic component of volatility we use is given by

$$\widehat{\eta}_{\phi_1,\phi_2}^{ret} = \sum_{i=\lfloor\phi_1\kappa/\Delta\rfloor+1}^{\lfloor\phi_2\kappa/\Delta\rfloor} \sum_{j=1}^{\mathcal{T}} \left(\Delta_{j,i}^n x\right)^2 \Big/ \sum_{i=1}^{\lfloor\kappa/\Delta\rfloor} \sum_{j=1}^{\mathcal{T}} \left(\Delta_{j,i}^n x\right)^2, \tag{24}$$

where $0 \leq \phi_1 < \phi_2 < 1$ and $\mathcal{T}$ is some integer denoting the number of trading days used in the estimation. This estimator, possibly with truncation of the returns, has been used commonly in prior work, see e.g., Taylor and Xu (1997) and more recently Andersen et al. (2023).[7] We do

[7] An alternative to $\widehat{\eta}_{\phi_1,\phi_2}^{ret}$ that can potentially provide efficiency gains is the counterpart of $\widehat{\eta}_{\phi_1,\phi_2}^{ret}$ in which the high-frequency returns are standardized by same day measure of integrated volatility, see e.g., Boudt et al. (2011). We do not provide results for such alternative estimators for two reasons. First, as far as we are aware the theoretically properties of such estimators have not been analyzed in prior work. Second, since we use relatively short time

not perform truncation of the returns because the diffusive and jump volatility share the same intraday diurnal pattern per our assumption in Section 2. We present results on the real data for the truncated counterpart of $\widehat{\eta}^{ret}_{\phi_1,\phi_2}$ in Section 7.1.

We compare $\widehat{\eta}_{\phi_1,\phi_2}$ and $\widehat{\eta}^{ret}_{\phi_1,\phi_2}$ using the same time window of 50 days. That is, we set $\mathcal{T}$ to 50 days for $\widehat{\eta}^{ret}_{\phi_1,\phi_2}$ and we average $\widehat{\eta}_{\phi_1,\phi_2}$ over the same number of days. In Figure 4 we compare the precision of $\widehat{\eta}_{\phi_1,\phi_2}$ and $\widehat{\eta}^{ret}_{\phi_1,\phi_2}$ across the trading day. Since the time for computing the option prices is nontrivial, we report result on the basis of 100 replications only. As seen from Figure 4, the efficiency gains offered by the option data can be rather nontrivial, particularly towards the end of the trading day when $\widehat{\eta}_{\phi_1,\phi_2}$ is around five times more efficient than $\widehat{\eta}^{ret}_{\phi_1,\phi_2}$.

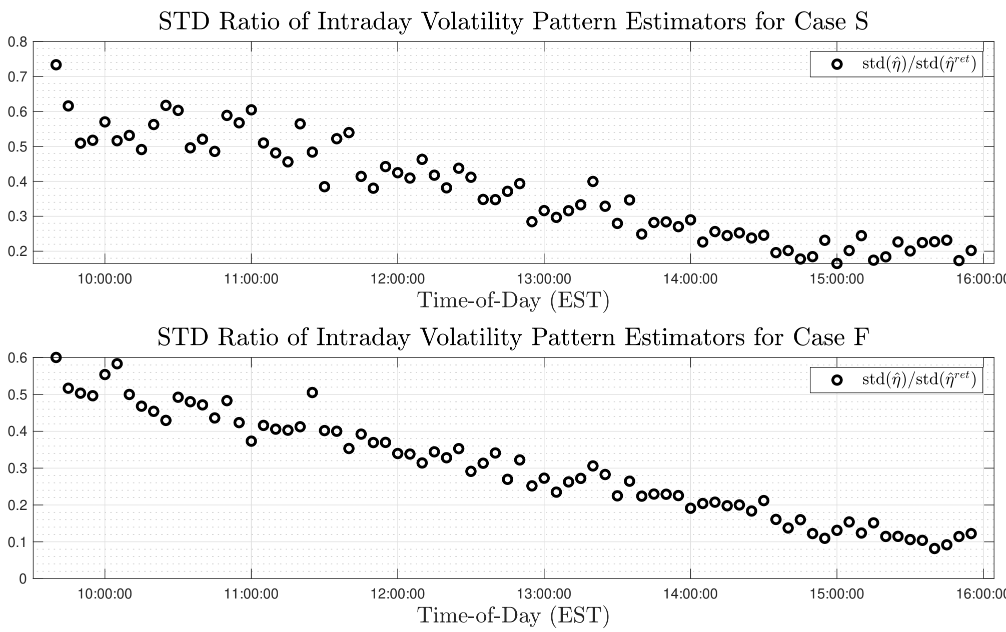

Figure 4: **Monte Carlo Results for Option- versus Return-based Estimator of Intraday Periodicity**. ϕ_1 and ϕ_2 correspond to consecutive observations on a 5-minute grid covering the time interval $9.35-15.55$ EST. Each dot on the plots corresponds to the ratio of standard deviations of the two estimators at each observation point during the trading day. The number of Monte Carlo replications is 100.

We note, however, that given the different source of the error in $\widehat{\eta}_{\phi_1,\phi_2}$ and $\widehat{\eta}^{ret}_{\phi_1,\phi_2}$, one can show that these estimators are asymptotically uncorrelated. Hence the optimal thing to do is to combine them. This is similar to the optimal use of high-frequency return data and option data for estimating spot volatility, see e.g., Todorov and Zhang (2022).

windows, the benefits from standardization with realized volatility are typically not very big (in the Monte Carlo experiments they result in around 5% reduction in the standard error of the estimates).

5 Empirical Application

5.1 Data

We apply the newly-developed estimators of volatility calendar effects to short-dated options written on the S&P 500 market index. Our sample covers the period from January 2, 2018 until December 31, 2020. The data is obtained from CBOE Data Shop and consists of best bid and best ask option quotes. Over our sample period, CBOE issued weeklies expiring on Monday, Wednesday and Friday of the week. Since in our analysis we use zero- and one-day tenor options (counting in business days), we thus look at intraday option data on every Friday which is not a holiday and consider the options on that day that expire either on the same day or on the next trading day. At each point in time and for each tenor, we determine an implied forward rate by using put-call parity for three distinct strikes with the smallest gap between call and put mid-quotes. Using the implied forward, we determine the moneyness of the options (defined as strike over forward) and keep only out-of-the-money options with non-zero bid quotes. We compliment the option data with intraday price records of the SPY exchange traded fund on the S&P 500 Index obtained from the NYSE Trade and Quote (TAQ) database. Our sampling frequency for both option and price data is every five minutes over the interval $9.35 - 15.55$ EST.

In Figures 5 and 6, we provide summary statistics for the option data used in our analysis. As seen from Figure 5, the number of strikes of the out-of-the-money short-dated options declines over the trading day as the options get closer to expiration. This effect is very pronounced for the zero-day options and is barely noticeable for the one-day options. Nevertheless, the median number of available strikes at 15.55 EST for the zero-day options is still nontrivial making possible the calculation of $QV_{t,T}$. Not surprisingly, the number of available strikes for the one-day options is significantly higher as they have one more day to expiration.

In Figure 6, we plot the volatility-adjusted moneyness range of the available options. We use at-the-money Black-Scholes implied volatility for computing the volatility adjustment of the moneyness range. As seen from the figure, the moneyness range for the one-day options is stable during the day. It is pretty wide on the negative side due to the well-known pricing of short-term left tail risk. The available range for the zero-day options is somewhat smaller and we note that it starts to shrink gradually around 14.30, with most of the change due to reduction in the available strikes for deep out-of-the-money puts. Nevertheless, the median strike range even at 15.55 EST is still relatively large, particularly when one takes into account the fact that Black-Scholes at-the-money implied volatility is higher than true volatility due to the risk premium embedded in

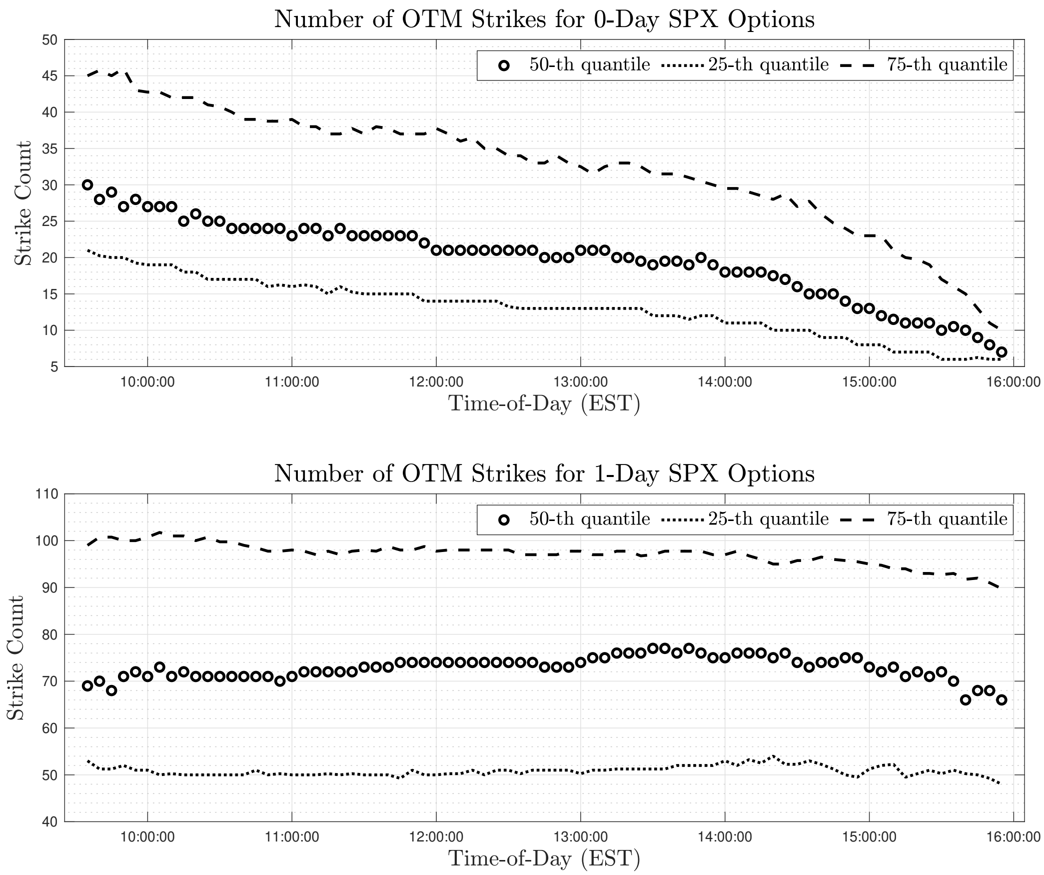

Figure 5: **Number of Strikes of S&P 500 Index Options for 0-Day (upper) and 1-Day (lower) Tenor.** For each time of day, we report 25-th, 50-th and 75-th quantile of the out-of-the-money strike counts across all days in the sample on a 5-minute grid covering the time interval $9.35 - 15.55$ EST.

it.[8]

5.2 Empirical Results

Using the available data, we compute the risk-neutral variance measures and form our estimates of the periodic component of volatility. In order to minimize the effect of occasional strike gaps in the data, we conduct linear interpolation in Black-Scholes implied volatility space to create option prices on equidistant strike grid with mesh of five and use these options in the calculation of $\widehat{QV}_{t,T}$. Note that the standard gap between observed strikes is five and in this sense the interpolation is

[8]The observed time-of-day patterns in Figures 5 and 6 of the number of options and the volatility-adjusted moneyness are related to the scaling laws of the Itô semimartingale increments over small time scales and to the properties of the jump compensator. Similar patterns, particularly the dependence of the strike count on the time of day, are observed in our Monte Carlo experiments as well.

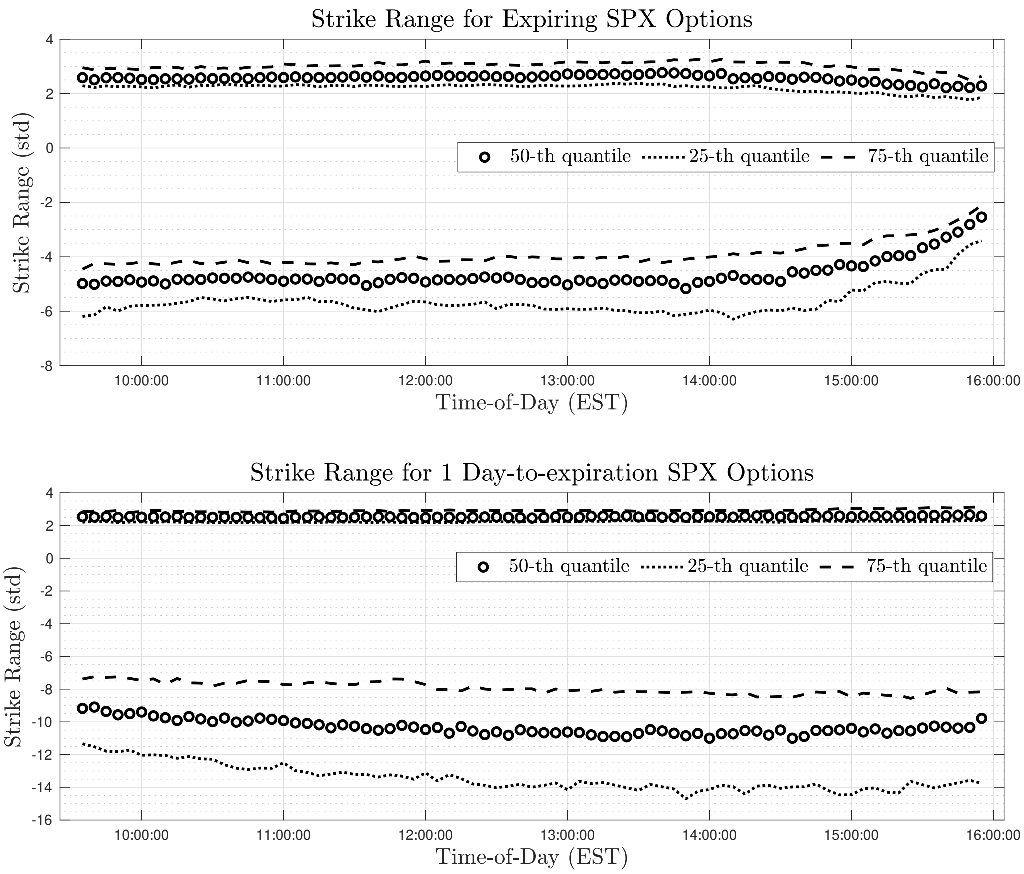

Figure 6: **Moneyness Range of S&P 500 Index Options for 0-Day (upper) and 1-Day (lower) Tenor.** For each time of day, we report 25-th, 50-th and 75-th quantile of the volatility-adjusted moneyness across all days in the sample on a 5-minute grid covering the time interval $9.35 - 15.55$ EST. The moneyness is volatility-adjusted using Black-Scholes at-the-money implied volatility.

minimal.[9] We further remove from the analysis pairs (t, T) with less than five observed out-of-the-money options. Finally, we make a finite-sample adjustment to $\widehat{\eta}_\phi$ that makes the estimate monotonic as a function of ϕ (recall that the estimand of $\widehat{\eta}_\phi$ is a decreasing function of ϕ). Mainly, starting from the end of the trading day (for which the precision of the estimation is highest), we modify iteratively the estimate of $\widehat{\eta}_\phi$ at observation times by taking the maximum of the original estimate and the estimate at the following observation time.

[9]We also experimented with interpolation at strike gaps of 1, with the results being essentially identical to the ones reported here. As an additional robustness check, we further experimented by performing bias correction for the tail truncation error using the expression for this bias given in (14) and the estimation of the tail decay parameters as in Bollerslev and Todorov (2014). Such bias correction had again negligible effect on the estimation and hence was performed only as a robustness check.

We estimate intraday volatility pattern on a yearly basis, i.e., by taking time series averages of $\widehat{\eta}_{\phi_1,\phi_2}$ over each of the year in the sample. The estimates are plotted in Figure 7. We can make several observations about the reported estimates. First, consistent with our simulation results, the option-based estimates at the beginning of the day appear noisier than the ones for later on in the trading day. Second, the estimated intraday volatility pattern has the familiar U-shape with volatility being higher at market open and market close relative to the middle of the trading day. Third, we do note some variation in the diurnal pattern over the three years in our sample. In particular, we can note a much higher estimate of volatility at 15.55 EST in 2020 than in the previous two years.

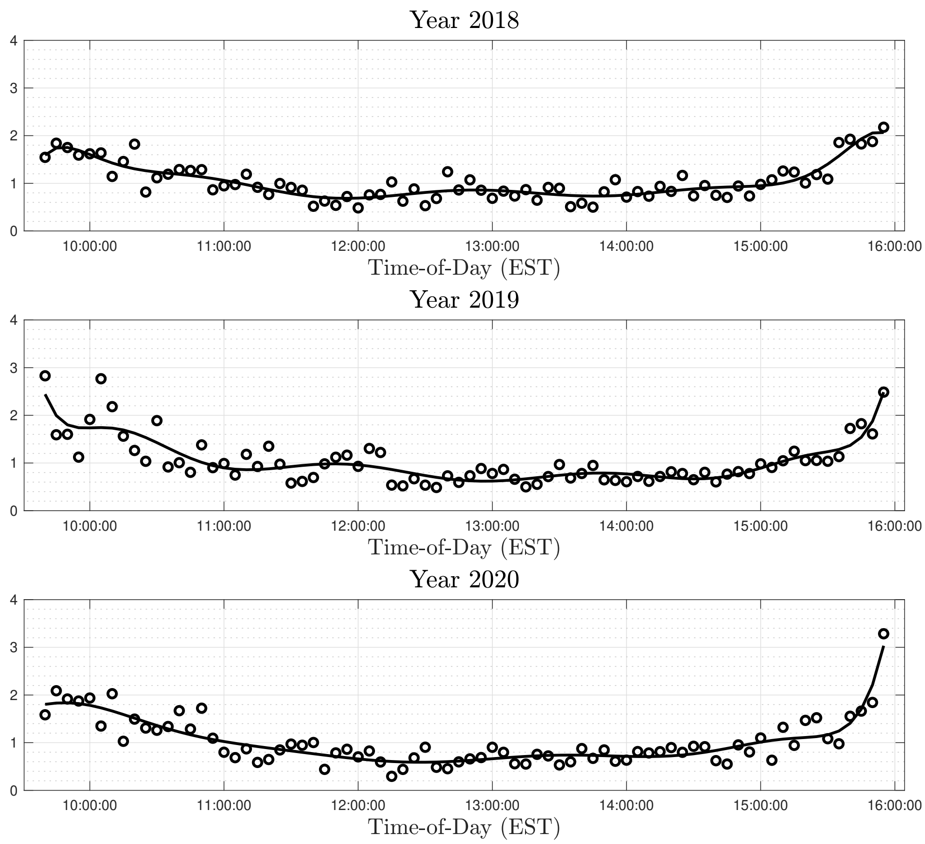

Figure 7: **Intraday Periodic Volatility Pattern of S&P 500 Index Volatility**. For each time of day, we report the time series average of the estimate of $\widehat{\eta}_{\phi_1,\phi_2}$, for ϕ_1 and ϕ_2 corresponding to consecutive observations on a 5-minute grid covering the time interval $9.35 - 15.55$ EST. The estimates are standardized by dividing by their average value across the times-of-day. The solid lines correspond to a tenth-order polynomial fit to the time-of-day estimates.

Overall, the reported estimates of η from the short-dated options illustrate the ability of such data to extract information for various volatility calendar effects. The recent introduction in 2022 of daily expiration cycle for the S&P 500 index options (and options written on other indices) should facilitate the application of such an analysis at a much more refined level. This can help uncover time-variation in volatility calendar effects that has been difficult or impossible to do with return data alone.

6 Conclusion

In this paper we propose an option-based nonparametric estimator of the deterministic periodic component of volatility. The estimator is based on short-dated options written on the underlying asset, expiring on the same or the following trading day. Unlike existing nonparametric methods for estimating the periodic component of volatility from high-frequency returns, the option-based method does not require the use of long time series of data (and the associated long-span asymptotics and assumptions needed for it). Instead, it relies on short-time asymptotics and options with two different times-to-maturity to disentangle the stochastic component of volatility from its deterministic periodic component. We derive the rate of convergence and an associated CLT for our estimator. A Monte Carlo study and an empirical application using S&P 500 index options show the applicability of the newly-developed estimation procedure.

7 Appendix

7.1 Jump-Robust Intraday Volatility Patterns

As mentioned in the main text, the intraday volatility pattern estimator developed in the paper relies on an assumption that the jump intensity exhibits the same intraday pattern as the diffusive volatility. In this section we provide empirical evidence using both options and stock returns in support of such an assumption. Towards this end, we introduce intraday volatility pattern estimates built from jump-robust volatility estimators. More specifically, we define

$$\widehat{SV}_{t,T} = -\frac{2}{\widehat{u}_{t,T}^2} \log|\widehat{\mathcal{L}}_{t,T}(\widehat{u}_{t,T})|, \tag{25}$$

where

$$\widehat{\mathcal{L}}_{t,T}(u) = 1 - (u^2 + iu) \sum_{j=2}^{N_{t,T}} e^{iu[\log(K_{t,T}(j-1)) - \log(X_t)]} \frac{\widehat{O}_{t,T}(K_{t,T}(j-1))}{K_{t,T}^2(j-1)} (K_{t,T}(j) - K_{t,T}(j-1)), \tag{26}$$

and

$$\widehat{u}_{t,T} = \widehat{u}_{t,T}^{(1)} \bigwedge \widehat{u}_{t,T}^{(2)},\ \widehat{u}_{t,T}^{(1)} = \inf\{u \geq 0.01 : |\widehat{\mathcal{L}}_{t,T}(u)| > 0.5\},\ \widehat{u}_{t,T}^{(2)} = \frac{\sqrt{2\log(1/0.05)}}{\sigma_{t,T}^{ATM}}, \tag{27}$$

for $\sigma_{t,T}^{ATM}$ being the non-annualized at-the-money implied volatility. As shown in Todorov (2019), this is a consistent estimator of $\mathbb{E}_t^{\mathbb{Q}}\left(\int_t^{t+T}\eta_{s/\kappa-\lfloor s/\kappa\rfloor}\sigma_s^2 ds\right)$, provided T is small. Using this estimator, we can construct a jump-robust counterpart of $\widehat{\eta}_{\phi_1,\phi_2}$. We denote this estimator with $\overline{\eta}_{\phi_1,\phi_2}$.

Similarly, we denote the truncated counterpart of $\widehat{\eta}^{\text{ret}}_{\phi_1,\phi_2}$ with $\overline{\eta}^{\text{ret}}_{\phi_1,\phi_2}$. That is, we use the truncated increment $\Delta_{j,i}^n x 1_{\{|\Delta_{j,i}^n x|\leq 3\Delta^{0.49}\sqrt{BV_j\wedge RV_j}\}}$ in $\overline{\eta}^{\text{ret}}_{\phi_1,\phi_2}$, where

$$BV_j = \frac{\pi}{2}\sum_{i=2}^{\lfloor\kappa/\Delta\rfloor}|\Delta_{j,i-1}^n x||\Delta_{j,i}^n x| \quad\text{and}\quad RV_j = \sum_{i=1}^{\lfloor\kappa/\Delta\rfloor}|\Delta_{j,i}^n x|^2. \tag{28}$$

In Figure 8, we compare the jump-robust estimates of the intraday volatility pattern with those in the main text that do not separate diffusive volatility from jumps in the estimation. We do this over the entire period 2018-2020 to reduce the effect from the estimation error. Starting with the option-based estimates, we can see only small differences. These differences are most apparent at the start of the trading day when the estimation error is much bigger. We can draw similar conclusion when comparing the two return-based estimators of the intraday volatility pattern. The differences between the two estimators appear small and there is no systematic pattern in these deviations along the trading day.

7.2 Assumptions and Proofs

7.2.1 Assumptions

The process x is defined on a filtered probability space $\left(\Omega,\mathcal{F},(\mathcal{F}_t)_{t\geq 0},\mathbb{Q}\right)$. We now state our assumptions for the dynamics of x which we need for the asymptotic analysis. Since we use different probability measures, to avoid confusion in the statements that follow, we will denote with $\mathbb{E}^{\mathbb{Q}}$ the expectation under $\mathbb{Q}$ and similarly $\mathbb{E}_t^{\mathbb{Q}}$ will be the $\mathcal{F}_t$-conditional expectation under $\mathbb{Q}$. We will not use superscripts for the counterparts of these expectations under $\mathbb{P}$. Our assumptions are as follows:

A1. *For $s\leq t$ in a neighborhood of 0, we have*

$$\mathbb{E}_s^{\mathbb{Q}}|\sigma_t^2-\sigma_s^2|^2 \leq C_s|t-s|, \tag{29}$$

and

$$\mathbb{E}_s^{\mathbb{Q}}\left|\int_{\mathbb{R}}(e^x-1-x)\nu_t(dx)-\int_{\mathbb{R}}(e^x-1-x)\nu_s(dx)\right|^2 \leq C_s|t-s|, \tag{30}$$

for some process C_t with càdlàg paths.

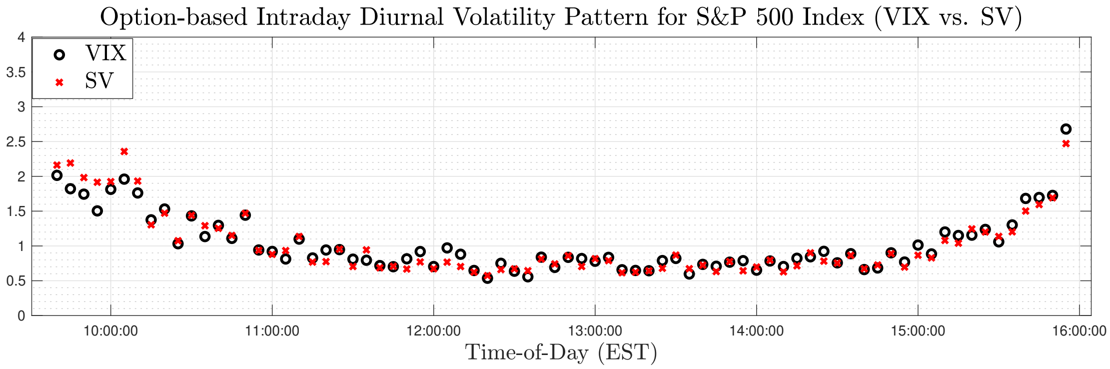

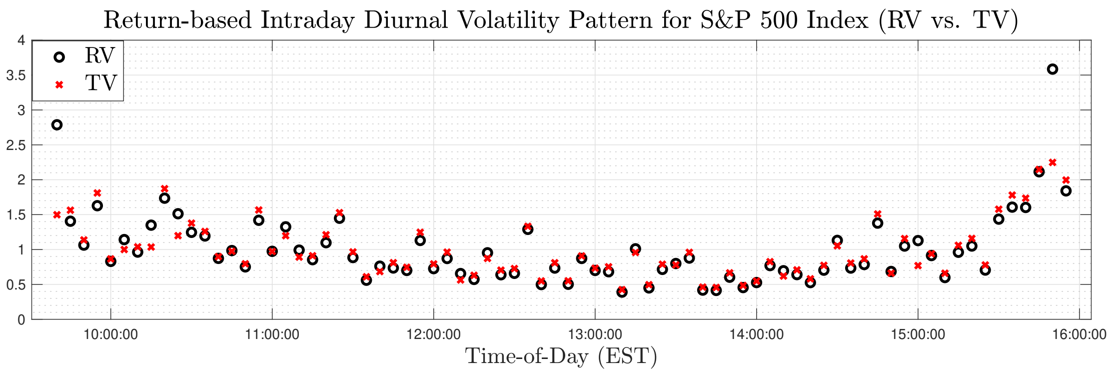

Figure 8: **Intraday Periodic Volatility Pattern of S&P 500 Index Volatility with and without Removal of Jumps**. For each time of day, we report the time series average of the estimate of $\widehat{\eta}_{\phi_1,\phi_2}$, for ϕ_1 and ϕ_2 corresponding to consecutive observations on a 5-minute grid covering the time interval $9.35 - 15.55$ EST. The estimates are standardized by dividing by their average value across the times-of-day. VIX and SV correspond to $\widehat{\eta}_{\phi_1,\phi_2}$ and $\overline{\eta}_{\phi_1,\phi_2}$, respectively. RV and TV correspond to $\widehat{\eta}^{\text{ret}}_{\phi_1,\phi_2}$ and $\overline{\eta}^{\text{ret}}_{\phi_1,\phi_2}$, respectively.

A2. *For t in a neighborhood of 0, there exist $\mathcal{F}_t^{(0)}$-adapted random variables C_t and $\bar{t} > t$ such that for $s \in [t, \bar{t}]$:*

$$\mathbb{E}_t^{\mathbb{Q}}|\alpha_s|^4 + \mathbb{E}_t^{\mathbb{Q}}|\sigma_s|^6 + \mathbb{E}_t^{\mathbb{Q}}(e^{4|x_s|}) + \mathbb{E}_t^{\mathbb{Q}}\left(\int_{\mathbb{R}}(e^{3|x|}-1)\nu_s(dx)\right)^4 < C_t. \tag{31}$$

A3. *For $i = 1, ..., n$, the log-strike grids $\{k_{i,0}(j)\}_{j=1}^{N_{i,0}}$ and $\{k_{i,1}(j)\}_{j=1}^{N_{i,1}}$ are $\mathcal{F}^{(0)}$-adapted and we have*

$$c_{t_i}\delta \leq k_{i,l}(j) - k_{i,l}(j-1) \leq C_{t_i}\delta, \quad l = 0, 1, \quad \text{as } \delta \downarrow 0, \tag{32}$$

where δ is a deterministic sequence, and c_t and C_t are $\mathcal{F}^{(0)}$-adapted processes with càdlàg paths with $\inf_t c_t > 0$. In addition, for some arbitrary small $\zeta > 0$:

$$\sup_{j:|k_{i,l}(j)-x_{t_i}|<\zeta}\left|\frac{k_{i,l}(j)-k_{i,l}(j-1)}{\delta} - \psi_{i,l}(k_{i,l}(j-1)-x_{t_i})\right| \xrightarrow{\mathbb{P}} 0, \quad l = 0, 1, \quad \text{as } \delta \downarrow 0, \tag{33}$$

where $\psi_{i,l}(k)$ are $\mathcal{F}^{(0)}$-adapted functions which are continuous in k at 0.

A4. *We have $\epsilon_{i,l}(j) = \zeta_{i,l}(k_{i,l}(j) - x_{t_i})\bar{\epsilon}_{i,l,j}O_{i,l}(j)$ for $l = 0, 1$, where for k in a neighborhood of zero, we have $|\zeta_{i,l}(k) - \xi_{i,l}(0)| \leq C_{t_i}|k|^{\iota}$, for some $\iota > 0$ and $C_t < \infty$ being an $\mathcal{F}^{(0)}$-adapted process with càdlàg paths. The two sequences $\{\bar{\epsilon}_{i,0,j}\}_{j=1}^{N_{i,0}}$ and $\{\bar{\epsilon}_{i,1,j}\}_{j=1}^{N_{i,1}}$ are defined on $\mathcal{F}^{(1)}$, are i.i.d. and independent of each other across $i = 1, ..., n$, and of $\mathcal{F}^{(0)}$. We further have $\mathbb{E}(\bar{\epsilon}_{i,l,j}|\mathcal{F}^{(0)}) = 0$, $\mathbb{E}((\bar{\epsilon}_{i,l,j})^2|\mathcal{F}^{(0)}) = 1$ and $\mathbb{E}(|\bar{\epsilon}_{i,l,j}|^{\kappa}|\mathcal{F}^{(0)}) < \infty$, for some $\kappa \geq 4$ and $l = 0, 1$.*

7.2.2 Proof of Theorem 1

We will make use of the following lemma in the proof:

Lemma 1. *Assume A and C1 hold. There exists $\mathcal{F}_t^{(0)}$-adapted random variables C_t and $\bar{t} > 0$ that do not depend on T such that for $T < \bar{t}$, we have*

$$O_{t,T}(K) \leq C_t\Bigg(TK^3 1_{\{\log(K/X_t)<-1\}} + TK^{-1}1_{\{\log(K/X_t)>1\}} + \left(\sqrt{T} \wedge \frac{T}{|\log(K/X_t)|}\right)1_{\{|\log(K/X_t)|<1\}}\Bigg), \tag{34}$$

$$|O_{t,T}(K_1) - O_{t,T}(K_2)| \leq C_t\left[\frac{T}{\log(K_2/X_t)^4} \bigwedge \frac{T}{\log(K_2/X_t)^2} \bigwedge 1\right]|K_1 - K_2|, \tag{35}$$

where $K_1 < K_2 < X_t$ or $K_1 > K_2 > X_t$. In addition, for $|\log(K/X_t)| \leq \sqrt{T}|\log(T)|$ and some $\iota > 0$ arbitrary small:

$$\left|O_{t,T}(K) - \sqrt{\eta_{t,T}}\sigma_t f\left(\frac{\log(K/X_t)}{\sqrt{\eta_{t,T}}\sigma_t}\right) - |k - x_t|\Phi\left(-\frac{|\log(K/X_t)|}{\sqrt{\eta_{t,T}}\sigma_t}\right)\right| \leq C_t T^{1-\iota}, \tag{36}$$

where $\eta_{t,T} = \int_t^{t+T}\eta_{s/\kappa-\lfloor s/\kappa\rfloor}ds$.

Proof of Lemma 1 The result in (34) for the cases $\log(K/X_t) < -1$ and $\log(K/X_t) > 1$ follows from the bound (7.5) of Lemma 1 of Todorov (2019) (note that Lemma 1 of Todorov (2019) is presented using the normalization $X_t = 1$). The result in (34) for the case $|\log(K/X_t)| < 1$ follows from combining the bounds in (7.6)-(7.8) of Lemma 1 of Todorov (2019). The result in (35) follows directly from the bound in (7.11) of Lemma 1 of Todorov (2019).

We are thus left with showing the result in (36). Denote with $O_{t,T}^c(K)$ corresponding to log-price $x_s^c = \sigma_t\int_t^s\sqrt{\eta_{u/\kappa-\lfloor u/\kappa\rfloor}}dW_u$, for $s \in [t, t+T]$, instead of x_s. Then, using Hölder inequality, we have that $|O_{t,T}(K) - O_{t,T}^c(K)| \leq C_t T^{1-\iota}$. Now, we note that η is a deterministic function. Hence,

$x^c_{t+T} - x^c_t$ is $\mathcal{F}_t$-conditionally normal with mean zero and variance $\sigma_t^2 \int_t^{t+T} \eta_{u/\kappa - \lfloor u/\kappa \rfloor} du$. From here, the proof follows exactly as that of the last one from Lemma 2 of Todorov (2019). □

We proceed with the proof of the theorem. We can make the decomposition

$$\widehat{QV}_{t,T} - QV_{t,T} = \widehat{Z}_{t,T} + R_{t,T}, \tag{37}$$

where

$$\widehat{Z}_{t,T} = \sum_{j=2}^{N_{t,T}} \frac{2}{K^2_{t,T}(j-1)} \epsilon_{t,T}(j-1)(K_{t,T}(j) - K_{t,T}(j-1)), \tag{38}$$

and

$$\begin{aligned} R_{t,T} = &-2\int_0^{K_{t,T}(1)} \frac{O_{t,T}(K)}{K^2} dK - 2\int_{K_{t,T}(N_{t,T})}^{\infty} \frac{O_{t,T}(K)}{K^2} dK \\ &+ 2\sum_{j=2}^{N_{t,T}} \int_{K_{t,T}(j-1)}^{K_{t,T}(j)} \left(\frac{O_{t,T}(K_{t,T}(j-1))}{K^2_{t,T}(j-1)} - \frac{O_{t,T}(K)}{K^2} \right) dK. \end{aligned} \tag{39}$$

Using the first two bounds of Lemma 1, we have

$$R_{t,T} = O_p\left((K^2_{t,T}(1) + K^{-2}_{t,T}(N_{t,T}))\kappa + \delta\sqrt{\kappa} \right). \tag{40}$$

Next, let us set $\widehat{Z}^{(l)}_\phi = \widehat{Z}_{t_i, T_i^l}$ for $i = \left\lfloor \frac{\phi\kappa}{\Delta} \right\rfloor$ and $l = 0, 1$, and write

$$\widehat{Z}^{(l)}_\phi = \sum_{j=2}^{N^{(l)}_\phi} z^{(l)}_{j,\phi}. \tag{41}$$

Using our assumption for the observation error and Lemma 1, we have

$$\mathbb{E}\left(z^{(l)}_{j,\phi} | \mathcal{F}^{(0)} \right) = 0, \quad \sum_{j=2}^{N^{(l)}_\phi} \mathbb{E}\left(|z^{(l)}_{j,\phi}|^{2+\iota} | \mathcal{F}^{(0)} \right) = O_p\left(\kappa^{3/2+\iota/2} \delta^{1+\iota} \right), \tag{42}$$

for some $\iota \in (0,1)$ and $l = 0, 1$. Therefore, we will have $\frac{1}{\sqrt{\delta}\kappa^{3/4}} (\widehat{Z}^{(1)}_\phi,\, \widehat{Z}^{(2)}_\phi) \xrightarrow{\mathcal{L}|\mathcal{F}^{(0)}} (Z_{\phi,1},\, Z_{\phi,2})$, by Theorem VIII.5.25 of Jacod and Shiryaev (2003), if we can establish the following convergence

$$\frac{1}{\delta\kappa^{3/2}} \sum_{j=2}^{N^{(l)}_\phi} \mathbb{E}\left(|z^{(l)}_{j,\phi}|^2 | \mathcal{F}^{(0)} \right) \xrightarrow{\mathbb{P}} \Sigma_{\phi,l}, \; l = 0, 1. \tag{43}$$

We establish the above convergence results in several steps by applying Lemma 1 and using assumptions A1 and A4. A direct application of assumption A4 yields

$$\mathbb{E}\left(|z^{(l)}_{j,\phi}|^2 | \mathcal{F}^{(0)} \right) = \frac{4}{K^4_{i,l}(j-1)} O^2_{i,l}(j-1) \zeta^2_{i,l}(k_{i,l}(j-1) - x_{t_i})(K_{i,l}(j) - K_{i,l}(j-1))^2. \tag{44}$$

Next, denote with $I^{\kappa}_{i,l}$, the set of integers j such that $|\log(K_{i,l}(j-1)/X_t)| \leq \sqrt{T^l_i}|\log(T^l_i)|$. Using the first bound of Lemma 1, the result in (44), assumption A3, and the fact that $O_{t,T}(K)$ is monotone increasing for $K < X_t$ and monotonically decreasing for $K > X_t$, we have

$$\sum_{j=2}^{N_\phi^{(l)}} \mathbb{E}\left(|z^{(l)}_{j,\phi}|^2 \big| \mathcal{F}^{(0)}\right) = \sum_{j\in I^{\kappa}_{i,l}} \mathbb{E}\left(|z^{(l)}_{j,\phi}|^2 \big| \mathcal{F}^{(0)}\right) + O_p\left(\delta\kappa^{3/2}/|\log(\kappa)|\right). \tag{45}$$

Using the first and third bounds of Lemma 1 and assumption A3, we can next write

$$\begin{aligned}\sum_{j\in I^{\kappa}_{i,l}} \mathbb{E}\left(|z^{(l)}_{j,\phi}|^2 \big| \mathcal{F}^{(0)}\right) = &\sum_{j\in I^{\kappa}_{i,l}} \frac{4}{K^4_{i,l}(j-1)}(\overline{O}^c_{i,l}(j-1))^2\zeta^2_{i,l}(k_{i,l}(j-1)-x_{t_i})(K_{i,l}(j)-K_{i,l}(j-1))^2 \\ &+ O_p\left(\delta\kappa^{2-\iota}|\log(\kappa)|\right),\end{aligned} \tag{46}$$

for some $0 < \iota < 1/2$ and where we use the following shorthand notation

$$\overline{O}^c_{t,T} = \sqrt{\eta_{t,T}}\sigma_t f\left(\frac{\log(K/X_t)}{\sqrt{\eta_{t,T}}\sigma_t}\right) + |k - x_t|\Phi\left(-\frac{|\log(K/X_t)|}{\sqrt{\eta_{t,T}}\sigma_t}\right). \tag{47}$$

Making use of assumption A3, assumption A4 for the function ζ as well as the first bound of Lemma 1, we can further expand

$$\begin{aligned}&\sum_{j\in I^{\kappa}_{i,l}} \frac{4}{K^4_{i,l}(j-1)}(\overline{O}^c_{i,l}(j-1))^2\zeta^2_{i,l}(k_{i,l}(j-1)-x_{t_i})(K_{i,l}(j)-K_{i,l}(j-1))^2 \\ &= \zeta^2_{i,l}(0)\sum_{j\in I^{\kappa}_{i,l}} \frac{4}{K^4_{i,l}(j-1)}(\overline{O}^c_{i,l}(j-1))^2(K_{i,l}(j)-K_{i,l}(j-1))^2 + O_p\left(\delta\kappa(\sqrt{\kappa}|\log(\kappa)|)^{1+\iota}\right),\end{aligned} \tag{48}$$

for some arbitrarily small $\iota > 0$. Next, making use of assumption A3, we can write

$$\begin{aligned}&\sum_{j\in I^{\kappa}_{i,l}} \frac{4}{K^4_{i,l}(j-1)}(\overline{O}^c_{i,l}(j-1))^2(K_{i,l}(j)-K_{i,l}(j-1))^2 \\ &= \sum_{j\in I^{\kappa}_{i,l}} \frac{4}{K^2_{i,l}(j-1)}(\overline{O}^c_{i,l}(j-1))^2(k_{i,l}(j)-k_{i,l}(j-1))^2 + O_p\left(\delta^2\kappa^{3/2}\right),\end{aligned} \tag{49}$$

and upon use of assumption A3 again and the definition of the set $I^{\kappa}_{i,l}$, we have further

$$\begin{aligned}\sum_{j\in I^{\kappa}_{i,l}} \frac{4}{K^2_{i,l}(j-1)}(\overline{O}^c_{i,l}(j-1))^2(k_{i,l}(j)-k_{i,l}(j-1))^2 = &\frac{4}{X^2_{t_i}}\sum_{j\in I^{\kappa}_{i,l}}(\overline{O}^c_{i,l}(j-1))^2(k_{i,l}(j)-k_{i,l}(j-1))^2 \\ &+ O_p\left(\delta\kappa^2|\log(\kappa)|\right).\end{aligned} \tag{50}$$

Now, we note that $X_{t_i} - X_0 = o_p(1)$ and $\zeta_{i,l}(0) - \zeta_{0,l}(0) = o_p(1)$ since X_t and $\zeta_{t,l}(0)$ are processes with càdlàg paths. Hence, we are left with the analysis of $\sum_{j\in I^{\kappa}_{i,l}}(\overline{O}^c_{i,l}(j-1))^2(k_{i,l}(j)-k_{i,l}(j-1))^2$.

Using assumption A3 and the càdlàg path of $\psi_{t,l}(0)$, we have

$$\sum_{j\in I_{i,l}^{\kappa}}(\overline{O}_{i,l}^{c}(j-1))^2(k_{i,l}(j)-k_{i,l}(j-1))^2=\psi_{0,l}(0)\delta\sum_{j\in I_{i,l}^{\kappa}}(\overline{O}_{i,l}^{c}(j-1))^2(k_{i,l}(j)-k_{i,l}(j-1))+o_p(\delta\kappa^{3/2}). \tag{51}$$

By applying first and second bound of Lemma 1 (which apply also to $\overline{O}_{t,T}^{c}(K)$) and assumption A3

$$\sum_{j\in I_{i,l}^{\kappa}}(\overline{O}_{i,l}^{c}(j-1))^2(k_{i,l}(j)-k_{i,l}(j-1))=\int_{-\sqrt{T_i^l}|\log(T_i^l)|}^{\sqrt{T_i^l}|\log(T_i^l)|}\left(\overline{O}_{t_i,T_i^l}^{c}(X_te^k)\right)^2dk+O_p\left(\sqrt{\kappa}|\log(\kappa)|^2(\delta^2+\delta\sqrt{\kappa})\right), \tag{52}$$

and we note that since $\delta\asymp\kappa^{\alpha}$ with $\alpha>1/2$, we have that $\sqrt{\kappa}|\log(\kappa)|^2(\delta^2+\delta\sqrt{\kappa})=o_p(\kappa^{3/2})$. Now, note that

$$\int_{|k|>\sqrt{T_i^l}|\log(T_i^l)|}\left(\overline{O}_{t_i,T_i^l}^{c}(X_te^k)\right)^2dk=o_p(\kappa^{3/2}). \tag{53}$$

We thus need to look at $\int_{\mathbb{R}}\left(\overline{O}_{t_i,T_i^l}^{c}(X_te^k)\right)^2dk$. From here, the result in (43) follows by a change of variable of integration and using the fact that the process σ_t has càdlàg paths.

In order to establish the result of the theorem, we are left with evaluating the difference $QV_{\lfloor\phi\kappa/\Delta\rfloor\Delta,(l+1)\kappa-\lfloor\phi\kappa/\Delta\rfloor\Delta}-QV_{\phi\kappa,(l+1-\phi)\kappa}$. We trivially have

$$QV_{\lfloor\phi\kappa/\Delta\rfloor\Delta,(l+1)\kappa-\lfloor\phi\kappa/\Delta\rfloor\Delta}-QV_{\phi\kappa,(l+1-\phi)\kappa}=O_p(\Delta),\ l=0,1. \tag{54}$$

Taking into account the rate condition in the theorem involving Δ, we get the result of the theorem.

7.2.3 Proof of Theorem 2

Using assumption A1 and the fact that the function η is deterministic, we have

$$\begin{aligned}\mathbb{E}_{\phi\kappa}^{\mathbb{Q}}&\left(\int_{\phi\kappa}^{\kappa}\eta_{s/\kappa-\lfloor s/\kappa\rfloor}\left(\sigma_s^2+2\int_{\mathbb{R}}(e^x-1-x)\nu_s(dx)\right)ds\right)\\&-\kappa\int_{\phi}^{1}\eta_sds\left(\sigma_{\phi\kappa}^2+\int_{\mathbb{R}}(e^x-1-x)\nu_{\phi\kappa}(dx)\right)=O_p(\kappa^2).\end{aligned} \tag{55}$$

Similar result holds for $QV_{\phi\kappa,(2-\phi)\kappa}$. From here, the result of the theorem follows.

References

Admati, A. and P. Pfleiderer (1988). A theory of intraday patterns: volume and price variability. *Review of Financial Studies 1*, 3–40.

Andersen, T. G. and T. Bollerslev (1997). Intraday periodicity and volatility persistence in financial markets. *Journal of Empirical Finance 4*(2-3), 115–158.

Andersen, T. G. and T. Bollerslev (1998). Deutsche mark–dollar volatility: intraday activity patterns, macroeconomic announcements, and longer run dependencies. *Journal of Finance 53*(1), 219–265.

Andersen, T. G., N. Fusari, and V. Todorov (2015a). Parametric Inference and Dynamic State Recovery from Option Panels. *Econometrica 83*, 1081–1145.

Andersen, T. G., N. Fusari, and V. Todorov (2015b). The Risk Premia Embedded in Index Options. *Journal of Financial Economics 117*, 558–584.

Andersen, T. G., N. Fusari, and V. Todorov (2017). Short-term market risks implied by weekly options. *The Journal of Finance 72*(3), 1335–1386.

Andersen, T. G., N. Fusari, V. Todorov, and R. T. Varneskov (2021). Spatial dependence in option observation errors. *Econometric Theory 37*(2), 205–247.

Andersen, T. G., T. Su, V. Todorov, and Z. Zhang (2023). Intraday periodic volatility curves. *Journal of the American Statistical Association*, 1–11.

Andersen, T. G., M. Thyrsgaard, and V. Todorov (2019). Time-varying periodicity in intraday volatility. *Journal of the American Statistical Association 114*(528), 1695–1707.

Bollerslev, T. and V. Todorov (2014). Time-varying jump tails. *Journal of Econometrics 183*(2), 168–180.

Boudt, K., C. Croux, and S. Laurent (2011). Robust estimation of intraweek periodicity in volatility and jump detection. *Journal of Empirical Finance 18*(2), 353–367.

Britten-Jones, M. and A. Neuberger (2000). Option prices, implied price processes, and stochastic volatility. *The journal of Finance 55*(2), 839–866.

Carr, P., H. Geman, D. Madan, and M. Yor (2003). Stochastic Volatility for Lévy Processes. *Mathematical Finance 13*, 345–382.

Carr, P. and L. Wu (2009). Variance risk premiums. *The Review of Financial Studies 22*(3), 1311–1341.

Christensen, K., U. Hounyo, and M. Podolskij (2018). Is the diurnal pattern sufficient to explain intraday variation in volatility? a nonparametric assessment. *Journal of Econometrics 205*(2), 336–362.

Duffie, D., J. Pan, and K. Singleton (2000). Transform Analysis and Asset Pricing for Affine Jump-Diffusions. *Econometrica 68*, 1343–1376.

Harris, L. (1986). A transaction data study of weekly and intradaily patterns in stock returns. *Journal of Financial Economics 16*(1), 99–117.

Heston, S. L. (1993). A closed-form solution for options with stochastic volatility with applications to bond and currency options. *The review of financial studies 6*(2), 327–343.

Hong, H. and J. Wang (2000). Trading and returns under periodic market closures. *Journal of Finance 55*(1), 297–354.

Jacod, J. and A. Shiryaev (2003). *Limit Theorems For Stochastic Processes* (2nd ed.). Berlin: Springer-Verlag.

Taylor, S. J. and X. Xu (1997). The incremental volatility information in one million foreign exchange quotations. *Journal of Empirical Finance 4*(4), 317–340.

Todorov, V. (2019). Nonparametric spot volatility from options. *The Annals of Applied Probability 29*(6), 3590–3636.

Todorov, V. and Y. Zhang (2022). Information gains from using short-dated options for measuring and forecasting volatility. *Journal of Applied Econometrics 37*(2), 368–391.

Wood, R. A., T. H. McInish, and J. K. Ord (1985). An investigation of transactions data for nyse stocks. *The Journal of Finance 40*(3), 723–739.